Int. J. Microgravity Sci. Appl., **33** (1) (2016) 330106
DOI: 10.15011/ijmsa.33.330106

IIIII Development of Boiling and Two-phase Flow Experiments on Board ISS IIIII
(Original Paper)

Development of Boiling and Two-phase Flow Experiments on Board ISS (Dissolved Air Effects on Subcooled Flow Boiling Characteristics)

Kenichiro SAWADA [1], Takashi KURIMOTO [2], Atsushi OKAMOTO [3], Satoshi MATSUMOTO [2], Hidemitsu TAKAOKA [2], Haruo KAWASAKI [4], Masahiro TAKAYANAGI [5], Yasuhisa SHINMOTO [6], Hitoshi ASANO [7], Osamu KAWANAMI [8], Koichi SUZUKI [9], Ryoji IMAI [10] and Haruhiko OHTA [11]

Abstract

Boiling is a very efficient mode of heat transfer because of the phase change involved and is a promising method for certain thermal management systems. However, the effects of gravity on two-phase flow phenomena in such systems have not been clarified in detail. To clarify these effects, boiling two-phase flow experiments onboard the Japanese Experiment Module "KIBO" have been proposed as an official Japanese Aerospace Exploration Agency project; this project concerns the effects of dissolved air on flow boiling heat transfer, which remains to be clarified in the case of a tube with an inner diameter of 4 mm. The abovementioned study involved conducting subcooled flow boiling experiments using various concentrations of dissolved air in perfluorohexane to clarify its effects on flow boiling heat transfer through a tube with an inner diameter of 4 mm. The excess temperature, boiling curve, and condensing heat transfer were determined and discussed. Consequently, dissolved air was demonstrated to affect boiling characteristics. In particular, dissolved air significantly affected the boiling curve in the low-heat-flux region: the boiling curve continuously decreased with increasing effective heat flux for mass fluxes of both G = 100 and G = 300 kg/m^{2}s. Moreover, dissolved air substantially affected the onset of boiling. These effects include decreasing the cluster radius required to form a nucleus. Furthermore, irrespective of the dissolved air concentration, no difference was observed among the boiling curves in the high-heat-flux region because of the fully developed flow regime, where a boiling curve determined according to the correlation proposed by Kandlikar effectively matched the experimental results in the case of a fluid-surface parameter F_{fl} of 1.7. This paper includes the contents of the proceedings of the 44th International Conference on Environmental Systems[1)].

Keyword(s): Dissolved Air, Perfluorohexane, Boiling, Two phase flow
Received 8 December 2015, Accepted 27 January 2016, Published 31 January 2016

1. Introduction

1.1 Project overview

Boiling is a very efficient mode of heat transfer because of the phase change involved and is a promising method for thermal management systems that handle bulk waste heat under high heat flux. However, the effects of gravity on two-phase flow phenomena and corresponding heat transfer characteristics have not yet been clarified in detail, despite many experiments covering both pool boiling and flow boiling have been conducted using various microgravity facilities and airplanes, as reviewed by Celata and Zummo[2)]. Experiments on boiling two-phase flow under microgravity conditions onboard the Japanese Experiment Module (JEM) "KIBO" in the International Space Station (ISS) have been proposed as part of an official Japanese Aerospace Exploration Agency project to clarify both heat transfer and flow characteristics under such conditions[3,4)].

The experimental theme is "Interfacial behaviors and heat transfer characteristics in boiling two-phase flow." These experiments provide a fundamental insight into the behavior of liquid–vapor flow and the heat transfer mechanism under microgravity conditions. This experience and knowledge will be applied in the design of high-performance space thermal management systems and clarify boiling two-phase flow characteristics. Scientific objectives are as follows:

1) To clarify the effects of gravity on heat transfer and critical heat flux in flow boiling.
2) To clarify regime maps and appropriately define dimensionless parameters for pressure drops, heat transfer coefficients, and critical heat flux under conditions where the gravity effect is observed.
3) To clarify the mechanisms of observed gravity effects on

1 Researcher, Research unit II, Research and Development Directorate, JAXA, 2-1-1 Sengen, Tsukuba, Ibaraki 305-8505, Japan
2 Associate Senior Engineer, Human Spaceflight Technology Directorate, JAXA, 2-1-1 Sengen, Tsukuba, Ibaraki 305-8505, Japan
3 Associate Senior Researcher, Research unit II, Research and Development Directorate, JAXA, 2-1-1 Sengen, Tsukuba, Ibaraki 305-8505, Japan
4 Associate Senior Engineer, SLATS Project Team, Space Technology Directorate I, JAXA, 2-1-1 Sengen, Tsukuba, Ibaraki 305-8505, Japan
5 Associate Principal Engineer, Human Spaceflight Technology Directorate, JAXA, 2-1-1 Sengen, Tsukuba, Ibaraki 305-8505, Japan
6 Assistant Professor, Dept. Aeronautics and Astronautics, Kyushu University, Nishi-ku, Fukuoka city, Fukuoka 819-0395, Japan
7 Associate Professor, Dept. Mechanical Engineering, Kobe university, Kobe city, Hyogo 657-8501, Japan
8 Associate Professor, Dept. Mechanical and System Engineering, University of Hyogo, Himeji city, Hyogo 671-2280, Japan
9 Professor, Dept. Mechanical Engineering, Tokyo University Science-Yamaguchi, Sanyo-Onoda, Yamaguchi 756-0084, Japan
10 Professor, Dept. Mechanical, Aerospace, and Materials Engineering, Muroran Institute of Technology, Muroran, Hokkaido 050-8585, Japan
11 Professor, Dept. Aeronautics and Astronautics, Kyushu University, Nishi-ku, Fukuoka city, Fukuoka 819-0395, Japan
(E-mail: sawada. kenichiro@jaxa.jp)

two-phase flow behaviors and heat transfer.

Engineering objectives are as follows:

1) To establish a database for liquid–vapor flow behaviors and corresponding flow boiling heat transfer in microgravity two-phase systems.
2) To provide fundamental information for developing large-scale two-phase thermal management systems for possible implementation in future spacecraft and earth-orbiting satellites on a large scale.

In the current project status, the critical design was completed using the engineering model (EM) test, thereby advancing the manufacture of the flight model (FM). A schematic of the EM is shown in **Fig. 1**. This loop comprises the following nine main components: two parallel magnetic drive gear pumps, two parallel 15 μm filters, a turbine flow meter, a preheater consisting of a copper tube, a metal heated tube made of copper tubing, a transparent heated tube made of Pyrex glass, two parallel adiabatic measuring tubes made of polycarbonate, a condenser, and an accumulator. Initially, the fluid is flowed in a liquid state by a pump while the liquid flow rate is measured by a turbine flow meter. The test section inlet temperature is controlled by a preheater, and the inlet pressure is controlled by an accumulator. The fluid is then heated to its boiling point and vaporized into two main test sections selected by valve operation: a metal heated tube and a transparent heated tube. The metal heated tube is used to obtain the local heat transfer coefficients distributed along the tube axis and the critical heat flux values, whereas the transparent heated tube is used to determine the direct relation between the measured heat transfer data and the observed liquid–vapor behavior. The heated fluid is then cooled to a subcooling condition in a condenser. Experiments are conducted using the Multi-purpose Small Payload Rack (MSPR) onboard the JEM "KIBO" in the ISS and the experimental apparatus developed for the MSPR. The experimental apparatus will be installed in the MSPR and subsequently launched in the HTV (H-IIA Transfer Vehicle), Dragon or Cygnus in early 2016.

The present experimental conditions on orbit are shown in **Table 1**. The outlet condition of these tubes is to be maintained at near-atmospheric pressure using the accumulator, where the saturation temperature is approximately 57 ℃ for perfluorohexane (PFH, C_6F_{14}), which is used as the working fluid. This PFH was obtained from Tokyo Chemical Industry (TCI). The chemical composition data obtained from gas chromatography–mass spectrometry (GC–MS) and gas chromatography with flame ionization detector (GC–FID) analyses of the TCI PFH sample is summarized in **Table 2**, and the physical properties of the TCI PFH under saturated conditions are shown in **Table 3**. Initially, Fluorinert (FC-72) was used as the working fluid; the TCI PFH was recently adopted instead of the FC-72 for official purposes, mainly because the component *n*-PFH purity of PFH exceeds that of FC-72. The PFH from TCI contains approximately 99.35 % *n*-PFH, whereas the FC-72 contains 73.7 % *n*-PFH. Because human safety is critical for this PFH, the lack of toxic

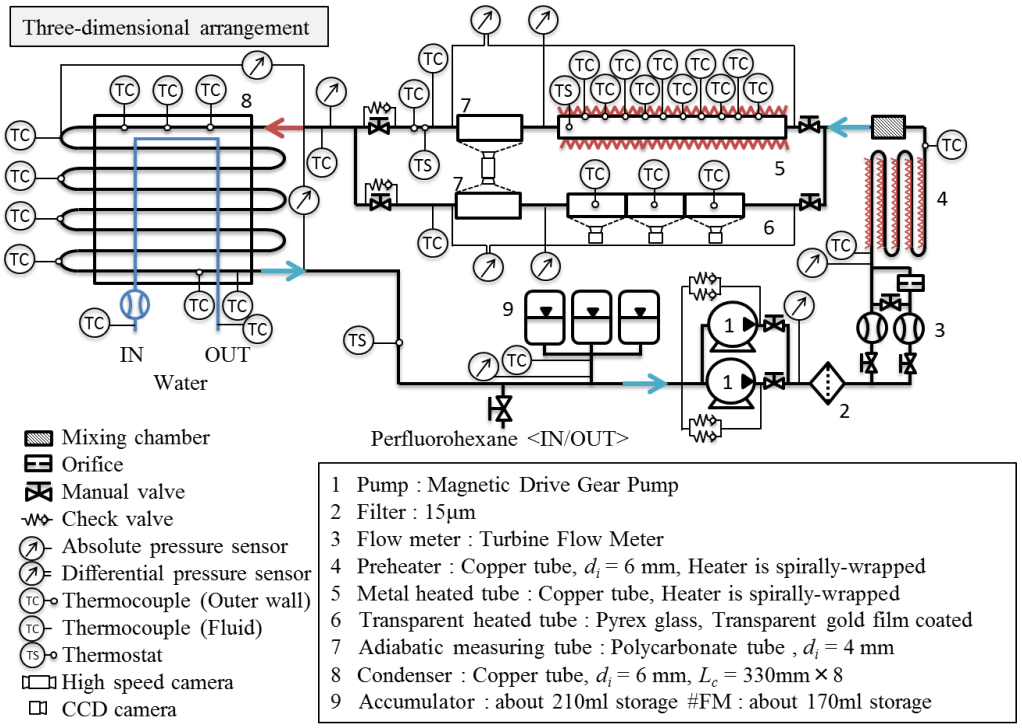

Fig. 1 Schematic view of the engineering model.

Table 1 Experimental conditions on orbit.

Working fluid	Perfluorohexane (degassed)
Test section inner diameter: d_i	4 mm
Mass flux: G	30–300 kg/m^{2}s
Maximum input power	250 W
Effective heat flux: q_{liq}	1–148 kW/m^2
Test section inlet subcooling: $\Delta T_{sub,i}$	0–30 K
Test section inlet vapor quality: x_i	0–0.9

Table 2 GC–MS/GC–FID profile of TCI PFH.

Structural assignment	Molecular weight	GC area [%]
n-Perfluorohexane	338	99.35
Perfluoro-2-methylpentane	338	0.14
C_5F_{12}	288	0.04
C_6F_{12} (perfluorocyclohexane)	338	Uncertain (<0.005%)
C_6F_{12} isomer (perfluorocyclohexane)	338	0.01
C_6HF_{13}	320	0.40
C_6HF_{13} isomer	320	0.02
Others	-	Uncertain (<0.04%)

Table 3 Physical properties of TCI PFH.

Temperature [°C]	25.0	57.0
Vapor pressure P_v [kPa]	29.5	101.6
Latent heat h_{lv} [kJ/kg]	92.62	83.54
Liquid density ρ_l [kg/m^3]	1691.4	1620.9
Gas density ρ_v [kg/m^3]	4.17	13.53
Liquid specific heat C_p [J/kg·K]	1046.4	1106.8
Liquid thermal conductivity k_l [mW/m·K]	57.97	54.16
Liquid viscosity [μPa·s]	664.4	412.8
Surface tension [mN/m]	11.39	8.43

byproducts from the PFH under experimental conditions should be confirmed on orbit. If the PFH were heated excessively, the fluid could generate a potentially toxic byproduct, perfluoroisobutylene (PFIB). Accordingly, NASA has already evaluated PFH in a thermal stress test to 450 °C, whereupon no trace of PFIB was observed under any of the investigated conditions after pyrolysis[5]. Accordingly, work has proceeded on a safety verification test using the newly manufactured safety verification model (SVM) to verify the influence of heat on the PFH and on the long-term performance of the loop components.

In this research, experimental test results are reported using the SVM as another objective of this verification test. This objective is explained in the next section.

1.2 Background and Objectives

PFH exhibits a high capacity for dissolved air. PFH can contain up to 25 times more dissolved air by volume than can water: 48 % air by volume can be dissolved in PFH under saturated conditions. Under equilibrium conditions, the dissolved air content can be described by Henry's law:

$$X = H * P_a \ , \tag{1}$$

where H is Henry's constant as a function of temperature, P_a is the dissolved air pressure, and X is the dissolved air concentration. Henry's constant for PFH was investigated by several researchers[6,7]. Dias and co-workers[6] investigated the solubility of oxygen in *n*-PFH and obtained the Henry's law coefficients as a function of temperature. The measured H values for oxygen in n-PFH are 0.205 and 0.345×10^{-5} moles/mole kPa at temperatures of 288 and 313 K, respectively. Moreover, You and co-workers[7] investigated the effect of dissolved gas content on pool boiling of FC-72. The measured H value for air in FC-72 is 5.4×10^{-5} moles/mole kPa over the temperature range from 31.5 to 59.5 °C, and dissolved gas influences the boiling incipient temperature above a certain molar fraction of the dissolved gas concentration (>0.005 moles/mole).

Despite the large capacity of PFH for dissolved air, the effects of dissolved air on pool boiling and flow boiling heat transfer in a tube with an inner diameter d_i of 4 mm remain to be clarified in detail. Notably, some researchers have attempted to clarify the effects of dissolved air by performing experiments with various fluids and under various test conditions[8-12]; these researchers confirmed some effects attributable to the presence of dissolved air. In particular, the subcooled flow boiling heat transfer under the saturated air condition has been reported to be either increased, decreased, or unaffected by the release of dissolved gas. Wei and co-workers[8] conducted pool boiling experiments using FC-72 and the surface of micro-pin-finned silicon chips. The gas-dissolved FC-72 exhibited a decrease in its boiling incipient temperature, and the heat-transfer performance in the low-heat-flux region exceeded that of degassed FC-72, although they exhibited similar performances in the high-heat-flux region.

Steinke and Kandlikar[9] investigated the effects of dissolved air on the flow boiling characteristics of water flowing through a tube with an inner diameter of 0.207 mm. In the case of dissolved oxygen content within the range from 1.8 to 8.0 ppm, boiling incipient surface temperatures varied for the levels of dissolved air, whereas the heat transfer coefficient decreased slightly at 8.0 ppm. The desorption of dissolved air from the insulating layer of bubbles on the heating surface was noted; this desorption had not been reported in the aforementioned investigation featuring 4 mm-diameter tubes. Conversely, all cases collapsed on the same boiling curve at high heat fluxes.

Cioncolini and co-workers[10] investigated the effects of dissolved air on subcooled and saturated flow boiling of water flowing through a tube with an inner diameter of 4.03 mm at

pressures from 177 to 519 kPa. They regarded the dissolved air in the water as a second-order effect, and the effects of dissolved gas clarified the apparent disagreement among results reported by different researchers.

Muller-Steinhagen and Epstein[11] investigated the effects of the dissolved gases on the subcooled flow boiling heat transfer of water and of heptane flowing through a tube with an inner diameter of 10.7 mm. The heat transfer varied substantially depending on the respective gas/liquid combination and the temperature of the liquid. The heat transfer coefficients for liquids containing dissolved gases always exceed those for degassed liquids due to the superposition of desorption and evaporation. Murphy and Bergles[12] investigated the dissolved gas effects on subcooled flow boiling heat transfer of Freon-113 flowing through a tube with an inner diameter of 0.5 inches. The dissolved gas effects were observed to increase the heat transfer substantially in partial boiling mode.

In the present work, we aimed to clarify the effects of dissolved air on the flow boiling heat transfer mechanism. Subcooled flow boiling experiments were conducted using a range of concentrations of dissolved PFH.

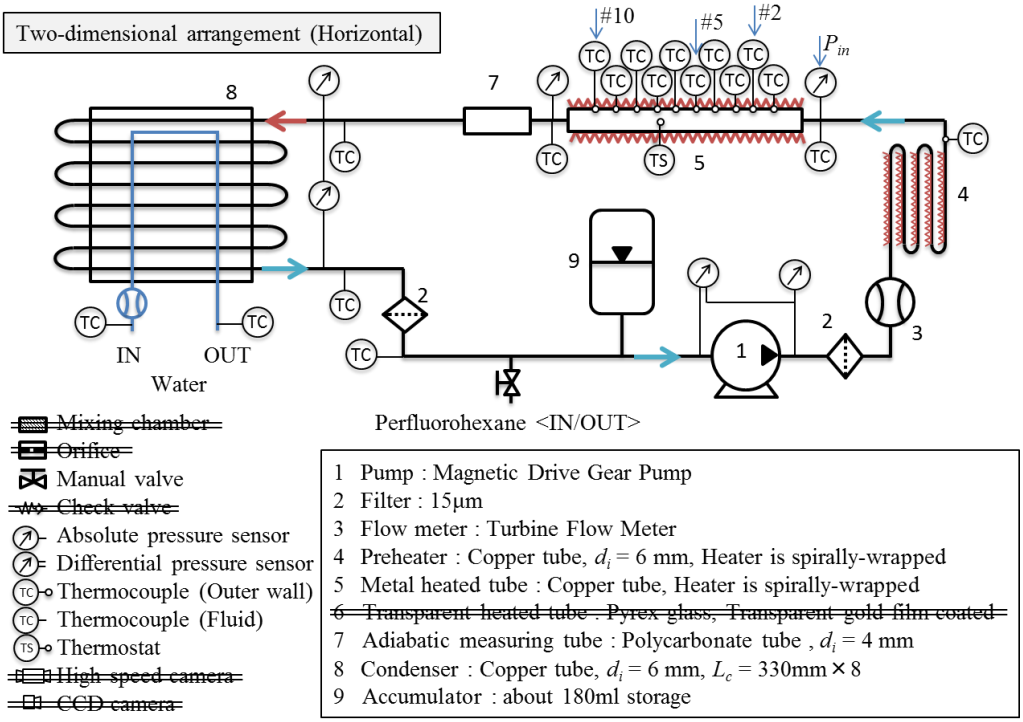

Fig. 2 Schematic view of the Safety Verification Model.

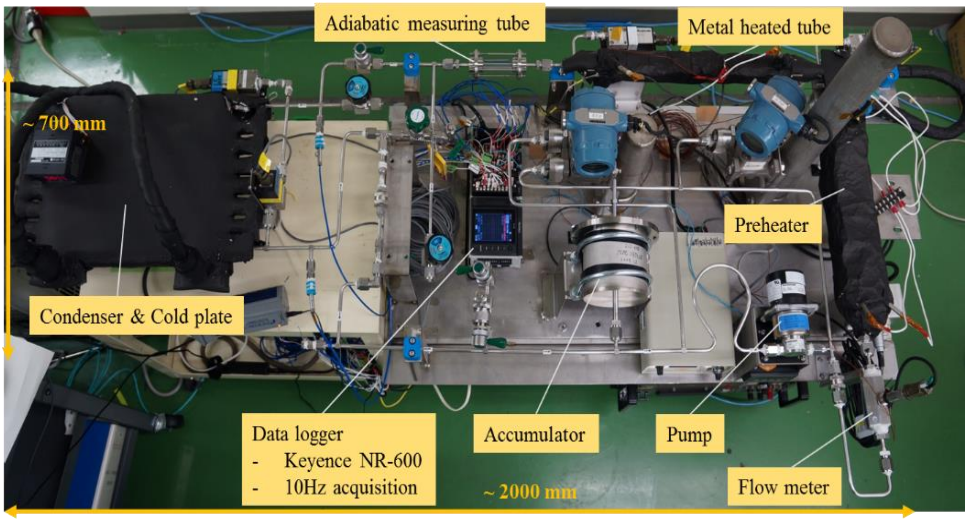

Fig. 3 External view of the Safety Verification Model.

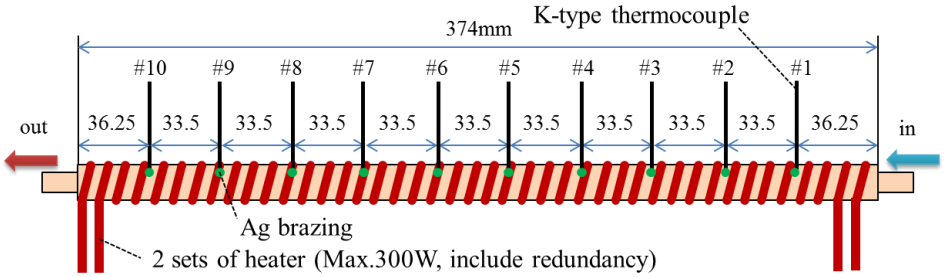

Fig. 4 Schematic of the metal heated tube.

Table 4 Experimental conditions.

Working Fluid	Perfluorohexane (TCI-PFH)
Dissolved gas concentration	Case 1. O_2: 2 ppm, N_2: 7 ppm*[1] Case 2. O_2: 6 ppm, N_2: 15 ppm Case 3. O_2: 7 ppm, N_2: 23 ppm Case 4. O_2: 16 ppm, N_2: 51 ppm Case 5. O_2: 28 ppm, N_2: 92 ppm Case 6. O_2: 38 ppm, N_2:124 ppm Case 7. O_2: 58 ppm, N_2:179 ppm Case 8. O_2: 82 ppm, N_2:199 ppm*[2] *[1]: degassed, *[2]: almost saturated
Test section inner diameter	4 mm
Mass flux	100 or 300 kg/m^{2}s
Effective heat flux: q_{liq}	1–50 kW/m^2
Test section inlet subcooling: ΔT_{sub}	15 ± 0.5°C
Cooling water temperature: T_{cw}	17 ± 0.5°C (ISS JEM cooling water simulated)
Cooling water flow rate: L_{cw}	40 L/min
Accumulator pressure: P_{ac}	105–130 kPa
Measuring frequency	10 Hz

2. Experimental apparatus

The experiments were conducted using the SVM. A schematic of the SVM is shown in **Fig. 2**, and an external view is shown in **Fig. 3**. The SVM configuration is almost equivalent to that of the EM, except for the absence of a transparent heated tube and a few pressure and temperature measurement points. The PFH fluid was circulated by the magnetic drive gear pump (1) and was mainly heated in the test section (5) comprising a copper tube with an inner dimeter of 4 mm. The inlet condition of the test section was controlled by both the accumulator and preheater; a schematic is shown in **Fig. 4**. The wall temperature of the test section was measured using 10 thermocouples located 0.5 mm from the inner heat transfer surface, whereas the fluid bulk temperature was calculated at various points by measuring the fluid temperature at the midpoint of the tube. The wall superheat and local heat transfer coefficients were calculated on the basis of the temperature measured at the metal heated tube in the outer wall. PFH flowed through the condenser (8) and was then supercooled. To prevent the solution from entering the main loop, the pipe and components were connected by a VCR fitting and Varian Torr Seal. Moreover, a sampling port made of isobutylene–isoprene rubber was used collect samples for the analysis of the dissolved gas.

3. Experimental conditions

A subcooled flow boiling experiment was conducted using various dissolved gas concentrations in PFH to clarify the effects of the dissolved gas on flow boiling heat transfer. The experimental conditions are shown in **Table 4**. The experiment was conducted under mass flux G = 100 or 300 kg/m^{2}s and inlet subcooling $\Delta T_{sub,I}$ = 15 K horizontally. To achieve the targeted inlet subcooling, the fluid was heated using the preheater; the effective heat flux was the preliminarily estimated value, which was calculated on the basis of heat loss during the single-flow test. The heat loss measurement results are shown in **Fig. 5**. The effective heat flux q_{liq} was estimated on the basis of the results of the single-phase flow experiment and is derived as follows:

$$q_{liq} = \frac{Q_i - Q_{loss}}{\pi d_i L} = \frac{Q_i - \left(Q_{i,s} - GA_{ts}C_{p,ts}\left(T_{ts,o} - T_{ts,i}\right)\right)}{\pi d_i L}, \qquad (2)$$

where Q_i is the heat input, $Q_{i,s}$ is the heat input at single-phase flow experiment, Q_{loss} is the estimated heat loss, d_i is the inner diameter of the test section, L is the test section length, $T_{ts,i}$ is the test section inlet fluid temperature, $T_{ts,o}$ is the test section outlet fluid temperature, $C_{p,ts}$ is liquid specific heat at average temperature of $T_{ts,i}$ and $T_{ts,o}$, and A_{ts} = $\pi d_i^2/4$. The q_{liq} value calculated using eq. (2) as a function of the wall temperature at the middle point (#5) of the test section was used to establish the test parameters used in the main experiment.

To control the dissolved gas concentration, we initially filled the SVM with fully degassed PFH, whereupon air was injected into the flowing loop via the isobutylene–isoprene rubber port using a 10 mL syringe, and gas concentration analyses were performed using gas chromatography in conjunction with a thermal conductivity detector (GC–TCD). The sample for the

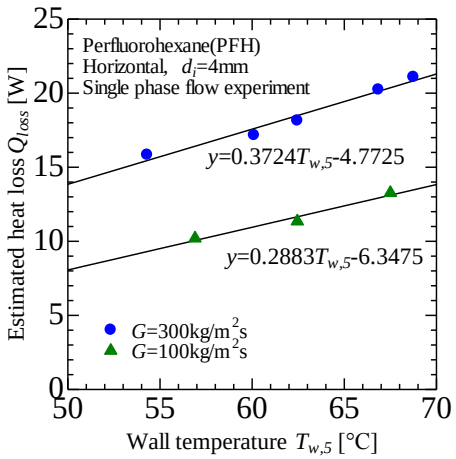

Fig. 5 Heat loss measurement results.

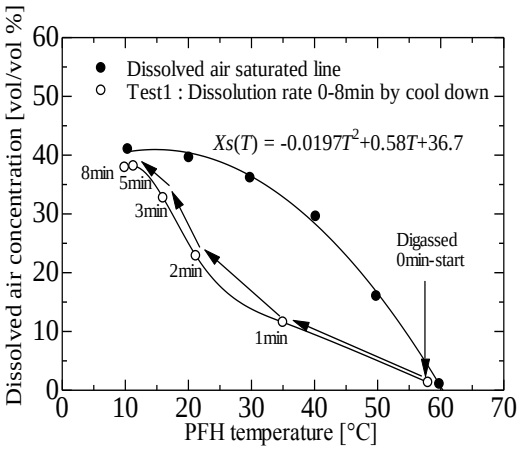

Fig. 6 Dissolved air concentration vs. fluid temperature.

analyses was withdrawn using a 100 μL syringe from the isobutylene–isoprene rubber sampling port.

Degassing exploits the increasing temperature and decreasing pressure of PFH in the stainless tank to reduce the dissolved gas concentration. Several degassing methods were considered, including freeze–pump–thaw degassing and decompression–heating degassing. Although the freeze–pump–thaw degassing method was capable of achieving a highly degassed condition, the decompression–heating degassing method was selected in view of operability. This method uses a large stainless tank, which is half-filled with PFH. The pressure in the upper gas area is reduced for approximately 30 s using the ACP15 compact dry roughing vacuum pumps, and PFH is subsequently heated for approximately 10 s. This operation is repeated approximately five times to reduce the concentration of dissolved air in PFH.

4. Results and Discussion

To clarify the effects of dissolved air on subcooled flow boiling heat transfer characteristics, we calculated the following parameters: excess temperature, boiling curve, and the condensing heat transfer; in addition, we studied the relationship between leakage points in the SVM and the ingress of dissolved air into PFH.

4.1 Dissolved air concentration characteristics

We confirmed the dissolved air concentration characteristics in PFH by conducting GC–TCD experiments. Initially, the saturated-dissolved-gas concentrations were confirmed as a function of PFH temperature, as shown in **Fig. 6** (black points). The saturated-dissolved-gas concentrations were approximately 40 vol/vol% at room temperature, whereby the saturated-dissolved PFH contained approximately 80 and 200 ppm of O_2 and N_2 gases, respectively. Conversely, the most extensively degassed PFH in the experiments contained approximately 1 ppm of both O_2 and N_2 gases. In addition, CO, CO_2, and H_2 gases were not detected because of their lower detection limits.

The dissolution rate between the air and PFH was excessive. An experiment using 50 mL PFH was conducted to clarify the dissolution rate between air and PFH. **Fig. 6** (white points) shows the time-dependent changes in the dissolved gas concentration in PFH as a result of its immediate cooling after being degassed. In this experiment, the interface between air and PFH in a beaker has a contact area of 0.001 mm^2. The dissolution rate can often be expressed by the Noyes–Whitney equation, whereby the dissolution rate between the air and PFH is derived as follows:

$$\frac{dX}{dt} = k \cdot S\{Xs(T) - X\} \tag{3}$$

where k is the dissolution coefficient, S is the contact area of the interface between the dissolving air and PFH, $Xs(T)$ is the dissolved air concentration under a steady-state condition, and X is the dissolved air concentration at that time. The dissolution coefficient k was confirmed by the experiment and exceeded 950 m^{-1}s^{-1}. The curve connecting the open circles in **Fig. 6** implies that PFH exhibits a very high dissolution rate; hence, preventing the ingress of atmospheric gases into the fluid loop is important.

4.2 Boiling characteristics

To clarify the effects of the dissolved air on the boiling characteristics of PFH, we calculated the changes in excess temperature and the boiling curve using experimental data.

Figure 7 shows the variation in wall temperature T_w as a function of the thermocouple number in the metal heated tube at G = 300 kg/m^{2}s for different values of dissolved gas concentrations in q_{liq} = 0.8 × 10^4 W/m^2 (low heat flux) and q_{liq} = 4.0 × 10^4 W/m^2 (high heat flux). In the low-heat-flux region, these wall temperatures exhibited different trends for different dissolved air concentrations. Greater dissolved air

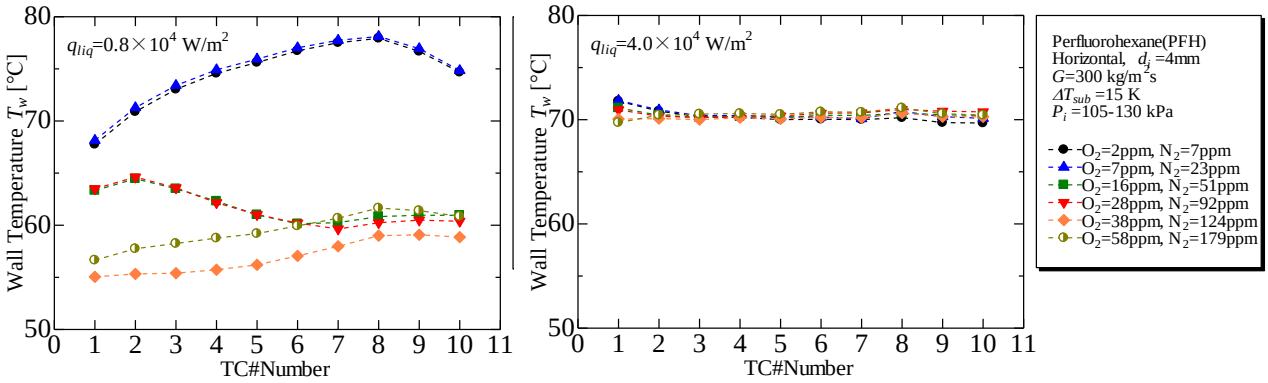

(a) q_{liq} = 0.8 × 10^4 W/m^2 (low-heat-flux case) (b) q_{liq} = 4.0 × 10^4 W/m^2 (high-heat-flux case)

Fig. 7 Variation of wall temperature as a function of the metal heated tube thermocouple number at a mass flux G of 300 kg/m^2s.

concentrations led to greater decreases in the wall temperature on the upstream side of the tube, indicating that the dissolved air led to the onset of nucleate boiling (ONB). Conversely, the dissolved air concentrations remained almost constant in the high-heat-flux region.

Figs. 8 and 9 show the boiling curves for G = 100 and G = 300 kg/m^2s at the test-section points farthest downstream and farthest upstream, respectively, (i.e., TC#10 (T_{wl0}) and TC#1 (T_{wl})). These two temperature measurement points were selected because different vaporization mechanisms may be encountered at different locations along the tube. In addition, the experimental results were compared to the predictions of the Kandlikar[13] correlation to confirm the discrepancies with this model reported by other researchers. Under the case of G = 300 kg/m^2s, a boiling curve was calculated using eq. (4); the results are shown in **Fig. 8**. In the fully developed boiling region, the wall superheat ΔT_e is derived as follows:

$$\Delta T_e = \frac{q_{liq}^{0.3}(Gh_{lv})^{0.7}}{1058F_{fl}\alpha_{l0}}, \tag{4}$$

where F_{fl} is the fluid surface parameter (F_{fl} = 1.0 in the case of water, F_{fl} = 1.63 in the case of R-134a, and F_{fl} = 3.50 in the case of neon, as proposed by Kandlikar[13]) and α_{l0} is the single-phase heat transfer parameter, which is calculated as follows:

$$\alpha_{l0} = \frac{Nu_{l0}\lambda_l}{d_i}, \tag{5}$$

where λ_l is the liquid thermal conductivity. Kandlikar proposed using the Gnielinski correlations for Nu_{l0} because these correlations appeared to effectively account for the Prandtl number (Pr_l) effect for different fluids. In the case of $0.5 \le Pr_l \le 2000$ and $2300 \le Re_{l0} < 10^4$, we computed Nu_{l0} using the correlation of Gnielinski[14], which is derived as follows:

$$Nu_{l0} = \frac{(\mathrm{Re}_{l0}-1000)(f/2)\mathrm{Pr}_l}{1+12.7(\mathrm{Pr}^{2/3}-1)(f/2)^{0.5}} \tag{6}$$

$$f = \left[1.58\ln(\mathrm{Re}_{l0}-3.28)\right]^{-2}, \tag{7}$$

$$\mathrm{Re}_{l0} = \frac{Gd_i}{\mu_l}, \tag{8}$$

where, Pr is the Prandtl number, Re is the Reynolds number, and μ_l is the liquid viscosity. These parameters were calculated for a temperature of 42°C (ΔT_{sub} = 15 K). The calculated values are as follows: Re_{l0} = 2314, f =0.01246, Nu_{l0} = 17.58, α_{l0} = 246.3 W/m^2K, h_{lv} = 83.826 kJ/kg. In this case, F_{fl} = 1.70 was used as the PFH fluid surface parameter.

In the case of the high-heat-flux region, **Fig. 8(b)** shows that the boiling curves effectively match the line of eq. (4) despite differences in the dissolved air concentrations because of the fully developed flow regime, such as the annular flow. Similarly, **Fig. 8(a)** shows that the boiling curves effectively match for lower dissolved air concentrations. Conversely, when the dissolved air concentration exceeds the half-saturation concentration, the boiling curves do not match the line of eq. (4). A slight deviation from the curve predicted by eq. (4) is observed despite the effective heat flux being the same; in addition, and boiling curve for higher dissolved air concentrations exhibits a lower excess temperature. **Figure 7** gives good understanding for this trends. In the case of air concentration at both 2 and 7 ppm of O_2, the wall temperature is higher than the boiling temperature at all points. It's a state of being heated to a temperature higher than boiling point without boiling. On the other hand, in the case of air concentration at both 38 and 58 ppm of O_2, the wall temperature is gradually

increase along the flow, and besides, **Fig. 8** shows the incipient jump at the onset of boiling was to a much lower wall temperature with dissolved air present. These are the evidence that onset of nucleate boiling is promoted by the the dissolved air present. In addition, the differences among these boiling curves decrease with increasing effective heat flux. An increase in the effective heat flux typically produces transitions in the flow regime. This transition was accelerated by the presence of dissolved air. The dissolved air affects the partial pressure in a direct fashion. Also, these trends were confirmed under variable mass flux conditions, as shown in **Fig. 9**. With respect to the ONB points, the required excess temperature for ONB decreased with increasing dissolved air concentration. The incipient jump is to a much lower wall temperature with dissolved gases present, reflecting the influence of the partial pressure of the dissolved gases. Accordingly, dissolved air substantially affects the ONB. The effect of the dissolved gases decreases the cluster radius required to form a nucleus. The relation between the cluster radius and gas concentration is derived as follows[15]:

$$r_e = \frac{2\sigma}{\eta' P_\infty + P_0 (X / X_S) - P_0} , \tag{9}$$

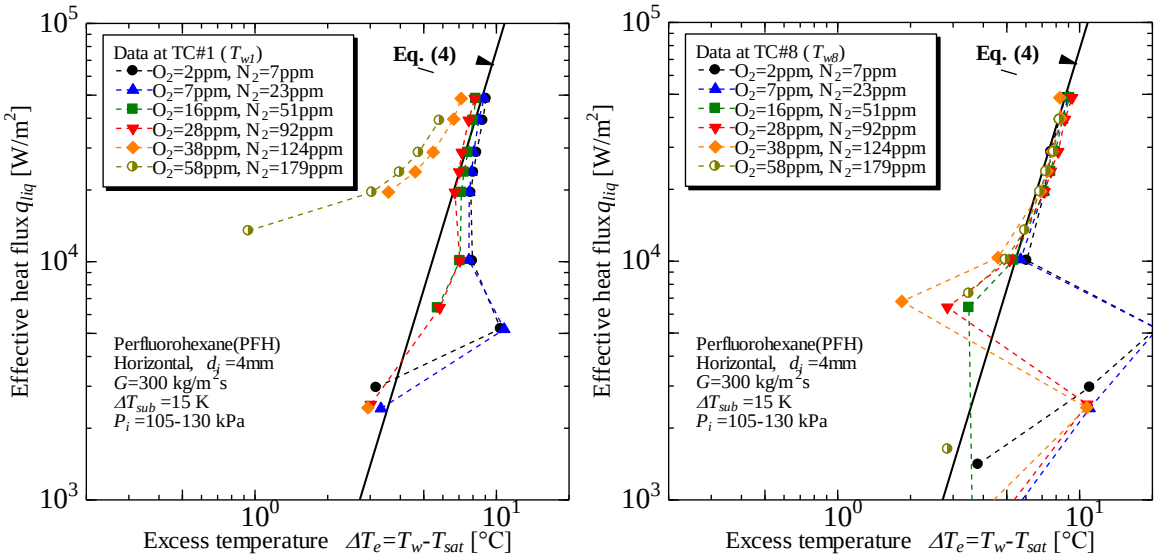

(a) Boiling curve at TC#1 (T_{w1}) . (b) Boiling curve at TC#8 (T_{w8}).

Fig. 8 Effective heat flux q_{liq} as a function of excess temperature $\Delta T_e = T_w - T_{sat}$ at G = 300 kg/m^{2}s.

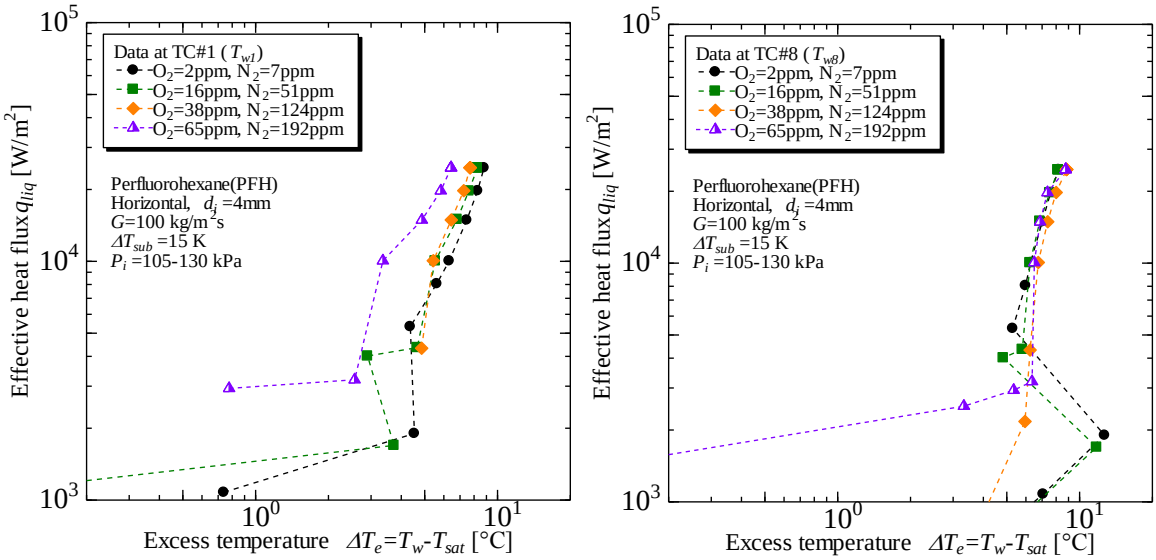

(a) Boiling curve at TC#1 (T_{w1}). (b) Boiling curve at TC#8 (T_{w8}).

Fig. 9 Effective heat flux q_{liq} as a function of excess temperature $\Delta T_e = T_w - T_{sat}$ at G = 100 kg/m^{2}s.

$$\eta' = \exp\left[\frac{\nu_{1l}(P_0 - P_\infty)}{RT_0} - X_2\right], \quad (10)$$

where r_e is the cluster radius, X/X_s is the air concentration in PFH, P_∞ is the outlet pressure of the cluster, P_0 is the inlet pressure of the cluster, and ν_{1l} is the surface tension.

Figure 10 shows the heat transfer coefficient for G = 100 and G = 300 kg/m^{2}s at both dissolved-air-degassed and almost-dissolved-air-saturated conditions. The heat transfer coefficients increase in proportion to approximately the 0.7th power of the effective heat flux; this relation is almost same between G = 100 and G = 300 kg/m^{2}s, as shown in **Fig. 10(a)**. In addition, a similar relation is confirmed for almost-dissolved-air-saturated and sufficiently high-heat-flux conditions in **Fig. 10(b)**.

Consequently, the half-air-saturation concentration was defined as the allowable air concentration during 1 year at the FM because the boiling curves under concentrations of less than the half-air-saturation concentration did not substantially differ. This definition according to the leakage rate is sufficient in view of the 200 day experimental period on orbit. We decided that the allowable leakage rate is 3.88 × 10^{-3} mL/s of ^{4}He at 271.2 kPaD (20 °C).

4.3 Condensation characteristics

To clarify the effects of dissolved air on the condensation characteristics, we calculated the overall convection coefficient U_c between the condenser and cold plate using the experimental data. This evaluation is simple because the local heat transfer coefficients could not be calculate because of insufficient measurement data. Clarifying these effects in detail would require measuring the local temperature and calculating the local heat transfer. The overall convection coefficient between

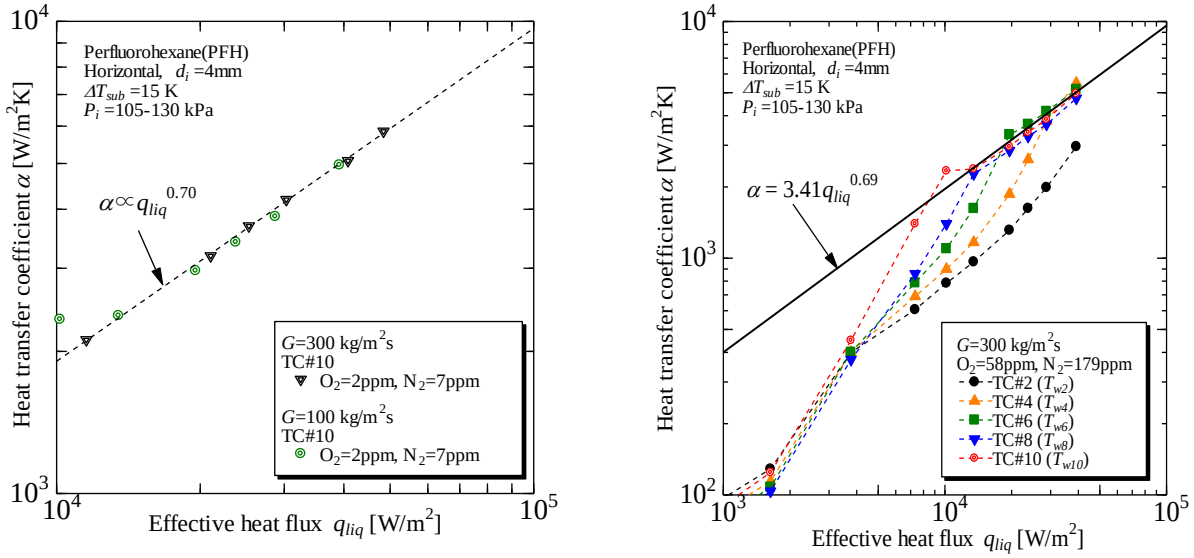

(a) G = 300kg/m^{2}s and G = 100kg/m^{2}s compared at degassed. (b) G = 300kg/m^{2}s at almost saturated.

Fig. 10 Heat transfer coefficient α as a function of effective heat flux q_{liq}.

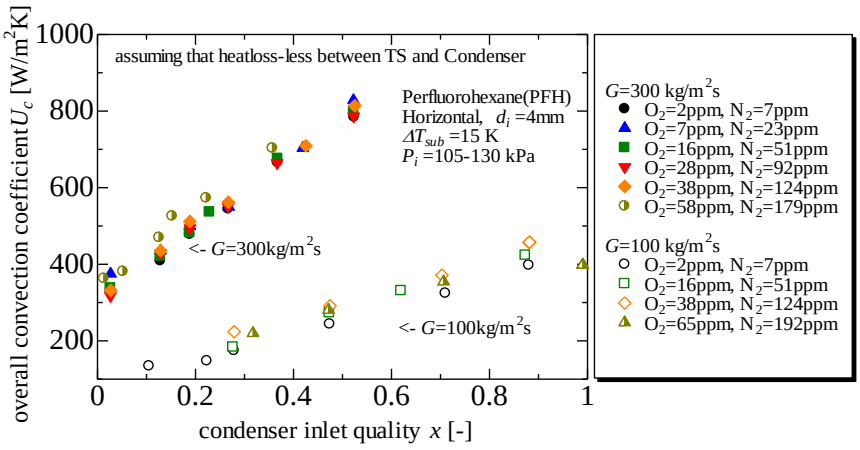

Fig. 11 Overall convection coefficient U_c as a function of condenser inlet quality x_c.

the condenser and cold plate is given as

$$U_c = \frac{Qcw}{A_c \Delta T_c} = \frac{L_{cw} C_{P,cw} \left(T_{cw,o} - T_{cw,i} \right)}{A_c \left\{ \frac{\Delta T1 - \Delta T2}{\ln(\Delta T1 / \Delta T2)} \right\}} \quad , \tag{11}$$

$$\Delta T1 = T_{ci,sat} - T_{cw,i} \quad ,$$

$$\Delta T2 = T_{c,o} - T_{cw,i} \quad ,$$

where L_{cw} is the cooling water flow rate, Q_{cw} is the heat exchange amount at the cooling water, A_c is the effective heat exchanger area, ΔT_c is the long mean temperature difference, $T_{ci,sat}$ is the saturation temperature at the condenser inlet, $T_{c,o}$ is the measured temperature at the condenser inlet, $T_{cw,i}$ is the measured temperature at the cooling water inlet, and $T_{cw,o}$ is the measured temperature at cooling water outlet.

In addition to this research, condenser design and analytical results have been reported by Imai et al.[16] and by Suzuki et al.[17]. As the main configuration in the condenser, eight rectangular copper tubes, which form a circular channel 6 mm in diameter, were directly connected by U-tubes and arranged in parallel on the cold plate.

Fig. 11 shows the relation between the overall convection coefficient and the condenser inlet quality. Despite the various concentrations of dissolved gases, none of these differences affects the overall convection coefficient U_c; the transition in varying condenser inlet quality is observed as a marked change because the heat transfer between the condenser tubes and the fluid occurred in a nearly subcooling state. As a possible effect of dissolved air on the condenser, the partial pressure of dissolved air in the two-phase fluid may affect the condensing heat transfer. However, the two-phase fluid had sufficiently cooled to a subcooled state in the first tube of the condenser, whereas seven tubes had cooled under a subcooling state. No dissolved air effects are evident in **Fig. 10** because the heat transfer represents a low proportion of the overall two-phase state.

4.4 Ingress of dissolved air into PFH

The amount of filled PFH in the SVM is approximately 704.5 mL. Air resistance was confirmed at a leakage rate of approximately 80 Pa/h after sufficient evacuation by the turbo molecular pump. At this leak rate, the dissolved air concentration showed virtually no variation over approximately 10 months: the O_2 concentration increased from 1 ppm to 3 ppm, whereas the N_2 concentration increased from 4 ppm to 10 ppm. This result indicates that the dissolution rate was reduced sufficiently through the use of VCR fittings and an isobutylene–isoprene rubber sampling port because these provisions reduce the contact area between PFH and air.

5. Conclusion

To clarify effects of dissolved air on the flow boiling heat transfer through a tube with an inner diameter of 4 mm, we conducted subcooled flow boiling experiments using various dissolved air concentrations.

The characteristics of the dissolved air are as follows:

I. The saturated dissolved air concentration $X_s(T)$ vol/vol percent was $X_s(T) = -0.0197\ T^2 + 0.58\ T + 36.7$ for 10 to 60°C.
II. The dissolution rate k between air and PFH exceeded 950 $m^{-1}s^{-1}$.
III. The dissolution rate was reduced sufficiently through the use of VCR fittings and an isobutylene–isoprene rubber sampling port.

The effects of dissolved air on boiling characteristic are as follows:

I. Dissolved air substantially affected the subcooled boiling in the low-heat-flux region; the boiling curve continuously decreased with increasing effective heat flux at both G = 100 and G = 300 kg/m^{2}s. Conversely, under the high-heat-flux region, despite the different dissolved air concentrations, no differences were observed among the boiling curves because of the fully developed flow regime.
II. Dissolved air substantially affected the onset of boiling and reduced the cluster radius required to form a nucleus. The incipient jump at the onset of boiling was to a much lower wall temperature with dissolved gases present, which influenced the partial pressure of dissolved air.
III. In the high-heat-flux region, a boiling curve calculated using the correlation proposed by Kandlikar matched the experimental results in the case of a fluid–surface parameter F_{fl} = 1.7.

The effects of dissolved air on the condensing heat transfer are as follows:

I. Irrespective of the dissolved air concentration, none of the differences affected the overall convection coefficient U_c or the transition with various condenser inlet quality x_c for both G = 100 and G = 300 kg/m^{2}s because the heat transfer included a low proportion of the overall two -phase state.

In a future study, we intend to conduct a detailed evaluation to clarify the effects of dissolved air in detail by increasing the number of measuring points. Moreover, we have planned experiment using various heating methods to confirm the effects of hysteresis.

Acknowledgments

The authors gratefully acknowledge the participation of all project members from Kyushu Univ., Kobe Univ., Univ. of Hyogo, Tokyo Univ. Sci. Yamaguchi, IHI Corporation, IHI Aerospace Co., Ltd., JAMSS, and JSF.

References

1) K. Sawada, T. Kurimoto, A. Okamoto, S. Matsumoto, H. Asano, O. Kawanami, K. Suzuki and H. Ohta: 44th International Conference on Environmental Systems proceedings (2014).
2) G.P. Celata and G. Zummo: J. multiphase Science and Technology, **21** (2009) 187.
3) K. Fujii, K. Masato, K. Kurimoto, H. Kawasaki, K. Sawada, K. Suzuki, H. Asano, O. Kawanami, R. Imai, Y. Shinmoto and H. Ohta: J. Physical Science and Application, **2** (2012) 71.
4) S. Baba, T. Sakai, K. Sawada, C. Kubota, Y. Wada, Y. Shinmoto, H. Ohta, H. Asano, O. Kawanami, K. Suzuki, R. Imai, H. Kawasaki, K. Fujii, M. Takayanagi and S. Yoda: J. Physics: Conference Series, **327** (2011) 012055.
5) W.A. Arnold, T.G. Hartman and J. McQuillen: J. Spacecraft and Rockets, **44** (2007) 94.
6) A.M.A. Dias, R.P. Bonifacio, I.M. Marrucho, A.A. H. Padua and M.F. Costa Gomes: J. Physical Chemistry Chemical Physics, **5** (2003) 543.
7) S.M. You, T.W. Simon, A. Bar-Cohen and Y.S. hong: J. Heat Transfer, **117** (1995) 687.
8) J.J. Wei, L.J. Guo and H. Honda: J. Heat and Mass Transfer, **41** (2005) 744.
9) M.E. Steinke and S.G. Kandlikar: J. Heat and Mass Transfer, **47** (2004) 1925.
10) A. Cioncolini, L. Santini and M.E. Ricotti: J. Experimental Thermal and Fluid Science: **32** (2007) 38.
11) H. Muller-Steinhagen, N. Epstein and A.P. Watkinson: Chemical Engineering and Processing, **23** (1988) 115.
12) R.W. Murphy and A.E. Bergles: Heat Transfer Laboratory Report No. DSR 71903-72 (1971).
13) S.G. Kandlikar: J. Heat Transfer, **113** (1991) 190.
14) V. Gnielinski: International Chemical Engineer, **16** (1976) 359.
15) S. van Stralen and R. Cole: Boiling Phenomena, Physical and Engineering Fundamentals and Applications, Hemisphere publishing corporation, **1** (1979) 81.
16) R. Imai, K. Suzuki, H. Kawasaki, C. Hong, H. Ishizuka, K. Fujii, Y. Shinmoto and H. Ohta: J. Jan. Soc. Microgravity Appl., **28** (2011) 109.
17) K. Suzuki, R. Imai, H. Kawasaki, C. Hong, H. Ishizuka, K. Fujii, Y. Shinmoto and H. Ohta: J. Jan. Soc. Microgravity Appl., **28**, (2011) 112.